

Chaotic bursting as chaotic itinerancy in coupled neural oscillators

Seung Kee Han

Department of Physics and BSRC, Chungbuk National University, Cheongju, Chungbuk 361-763, Korea

D. E. Postnov

Physics Department, Saratov State University, Astrakhanskaya Str. 83, Saratov 410026, Russia

(Received 7 February 2003; accepted 18 June 2003; published 22 August 2003)

We show that chaotic bursting activity observed in coupled neural oscillators is a kind of chaotic itinerancy. In neuronal systems with phase deformation along the trajectory, diffusive coupling induces a dephasing effect. Because of this effect, an antiphase synchronized solution is stable for weak coupling, while an in-phase solution is stable for very strong coupling. For intermediate coupling, a chaotic bursting activity is generated. It is a mixture of three different states: an antiphase firing state, an in-phase firing state, and a nonfiring resting state. As we construct numerically the deformed torus manifold underlying the chaotic bursting state, it is shown that the three unstable states are connected to give rise to a global chaotic itinerancy structure. Thus we claim that chaotic itinerancy provides an alternative route to chaos via torus breakdown. © 2003 American Institute of Physics. [DOI: 10.1063/1.1598691]

The central nervous system consists of billions of neurons and each of them are connected to thousands of other neurons by synapses. The complexity of the neural network has defied detailed analysis for the understanding of information processing in the brain. With the development of new experimental techniques, simultaneous measurement of hundreds to thousands of neurons now becomes possible. Together with computation modeling, it enables us to analyze the network activity. As a complex system, the emergent behavior of the network, like collective synchronous activity, multistability, and adaptation of the network will be very interesting to investigate. As chaotic bursting activity is also one of the most frequently observed dynamic neural activities, interest in the role of chaotic itinerant activity in information processing is now growing. Still we do not know much about this state. Therefore, the study of two coupled neural oscillator systems presented in this paper will shed light on the mechanism of its generation.

I. INTRODUCTION

Bursting activity has been observed in numerous neuronal systems¹ and cells.² In neuronal systems, it is a slow alternation between a sequence of fast repetitive *spiking* phases and *silent* nonspiking phases. Usually, the bursting activity occurs in chaotic form.³ Recent experimental results in neurobiology have renewed interests in the cooperative dynamical properties with a possible role of information processing in the brain.⁴ The role of chaotic bursting behavior on the information processing in neural system especially attracts the interest of theoreticians.⁵⁻⁷

A typical approach to bursting phenomena is based on systems with both *fast* and *slow* variables. For bursting behavior, the fast variables which are responsible for the firing activity should exhibit multistability, coexistence of a resting

state and a regular firing state, while the slow variable acts as a control parameter for fast dynamics. As the slow variable drives the fast dynamics from a parameter regime of the resting state to another parameter regime of the firing state, we observe bursting behavior. Recently, a systematic classification of mathematical models of bursting was presented based on the possible types of local or global bifurcations of fast dynamics.^{8,9}

An alternative mechanism of bursting behavior which does not utilize additional slow variables was proposed recently.¹⁰ It occurs in coupled systems as a consequence of mutual interactions between fast spiking neurons. In neuronal systems with phase deformation along the periodic limit cycle, weak diffusive coupling in one dynamic variable induces *dephasing* that leads to the antiphase, rather than in-phase, synchronization. It was observed by Sherman and Rinzel¹¹ and investigated in detail in Refs. 10 and 12. For strong diffusive coupling, due to mutual attraction toward each other, the in-phase solution becomes stable. For intermediate coupling, both the antiphase solution and the in-phase solution lose stability. Instead, a chaotic bursting state alternating between the transitory anti- and in-phase solutions and the nonfiring state is obtained. It is similar to *chaotic itinerancy* observed in high-dimensional systems.¹³⁻¹⁵

In high-dimensional systems, multistability with coexisting stable solutions occurs very frequently. As the stable solutions lose their stability with a change of the control parameter, the basins of attraction of each of the stable solutions are connected to each others through unstable manifolds. Then, an attracting state which traces out sequentially all of the destabilized *attractor ruins* emerges. This is a chaotic itinerant state. Due to the complexity of the high-dimensional system, however, no detailed illustrations that show how those unstable manifolds are organized to give rise to a global manifold structure of the chaotic itinerancy were presented up to now. Although the diffusively coupled two-oscillator system presented in this paper is relatively

simple, it exhibits chaotic itinerancy. Using this model, we will show how the manifolds of the unstable solutions organize to generate the global manifold structure of chaotic itinerancy.

In Sec. II we present a mathematical model of coupled neural oscillators. A bifurcation diagram showing the parameter regime of chaotic bursting is presented. Characteristics of chaotic bursting are presented in Sec. III. In Sec. IV, a numerical construction of manifold organization is presented. We explain how the manifolds of unstable solutions organize to give rise to a global chaotic itinerant attractor. Finally, in Sec. V we compare the route to chaotic itinerancy with the conventional route to chaos via destruction of the resonant torus.

II. COUPLED NEURAL OSCILLATORS

Our studies are based on the Morris–Lecar neuron model.¹⁶ It is a simplified version of the Hodgkin–Huxley model,¹⁷ which describes the spiking behavior and refractory properties of real neurons. Although the ML model has only two dynamical variables, it exhibits most of the dynamic features of the Hodgkin–Huxley model, including stimulus-dependent excitability and oscillatory behavior.

A two-coupled ML model is described by the equations for transmembrane voltage $v_{1,2}$ and activation variable $w_{1,2}$:

$$\begin{aligned} \frac{dv_{1,2}}{dt} &= -J_{\text{ion}}(v_{1,2}, w_{1,2}) + J_{1,2} + \gamma(v_{2,1} - v_{1,2}), \\ \frac{dw_{1,2}}{dt} &= f \frac{w_{\infty}(v_{1,2}) - w_{1,2}}{\tau_w(v_{1,2})}, \end{aligned} \quad (1)$$

where $J_{1,2}$ is the external current stimulus and γ is the coupling strength. For functions and parameters, see Ref. 18. The parameters in this equation are chosen such that a single oscillator has three fixed points, one stable, one saddle, and one unstable fixed point. A limit cycle surrounding the unstable fixed point is generated via subcritical Hopf bifurcation and disappears via homoclinic connection.¹¹

Let us consider the coupling of two identical oscillators with $J_1 = J_2$ and take the coupling strength γ varied. Because of the presence of a saddle point near the limit cycle, the diffusive coupling gives rise to the dephasing effect. Due to this effect, the antiphase synchronized solution, rather than the in-phase solution, is stable at weak coupling $\gamma \Rightarrow 0$.^{10–12} With an increase of γ , due to the nature of the diffusive coupling, the antiphase solution destabilizes. At large $\gamma > 0.5$, the two oscillators tend to oscillate in-phase. For intermediate coupling, the regions of stable out-of-phase solutions are overlapping with those of the antiphase and in-phase synchronization.

The two-parameter bifurcation diagram in Fig. 1 highlights a triangular region of chaotic bursting. It is bounded by one *SN* line and two *BC* lines. The line *SN* denotes a saddle-node bifurcation of the resonant phase cycles. Below this line, the antiphase synchronized solution is stable, while out-of-phase solutions are stable above this line. On the two lines *BC*, the chaotic bursting attractor undergoes boundary crisis,^{19,20} colliding with other limit cycles or their mani-

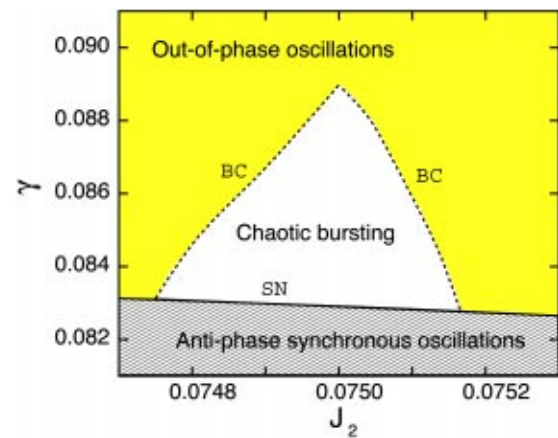


FIG. 1. (Color online) The region of chaotic bursting attractor is highlighted in two-dimensional parameter space, J_2 and γ . The *SN* and *BC* denote the saddle-node bifurcation and the boundary crisis, respectively. J_1 parameter is fixed as $J_1 = 0.075$.

folds. Therefore, within the triangular region, neither the antiphase solution nor the out-of-phase solutions are stable. For a full bifurcation diagram, see Ref. 21.

III. CHAOTIC BURSTING BEHAVIOR

As the coupling strength is increased to $\gamma = 0.08315$ along the line $J_2 = 0.075$ in Fig. 1, the regime of antiphase synchronous oscillation suddenly turns to a chaotic bursting regime. A typical time trajectory in the chaotic bursting regime is shown in Fig. 2. It is mixed with high amplitude oscillations representing repetitive spiking and nonspiking silent zones. Note that the interspike intervals are of order 10 (in arbitrary units), while the interbursting intervals are of order 1000. The interspike interval is quite constant over the region of chaotic bursting, but the interburst intervals depend on the coupling strength. As shown in the inset, the high-amplitude oscillations are also divided into two parts: one with high-amplitude oscillation and the other with medium-amplitude oscillation. Therefore, the bursting activity is composed of three different parts: a high-amplitude regular spiking, a medium-amplitude regular spiking, and a nonspiking small-amplitude oscillation (a *silent zone*).

Projection of phase portrait onto a phase plane (V_1, V_2) in Fig. 3(a) clarifies the characteristics of the three different parts. An in-phase synchronization, an antiphase synchronization, and a small-amplitude oscillation correspond to the

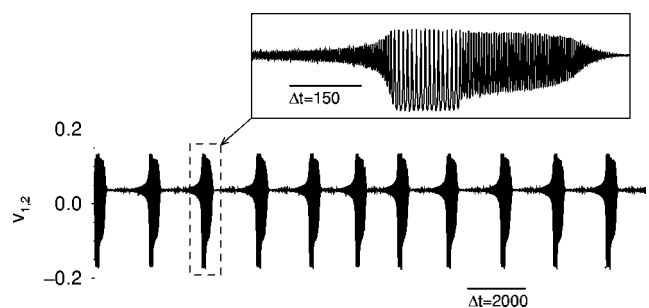


FIG. 2. A typical time trajectory of chaotic bursting behavior. One period of the burst activity is enlarged in the inset.

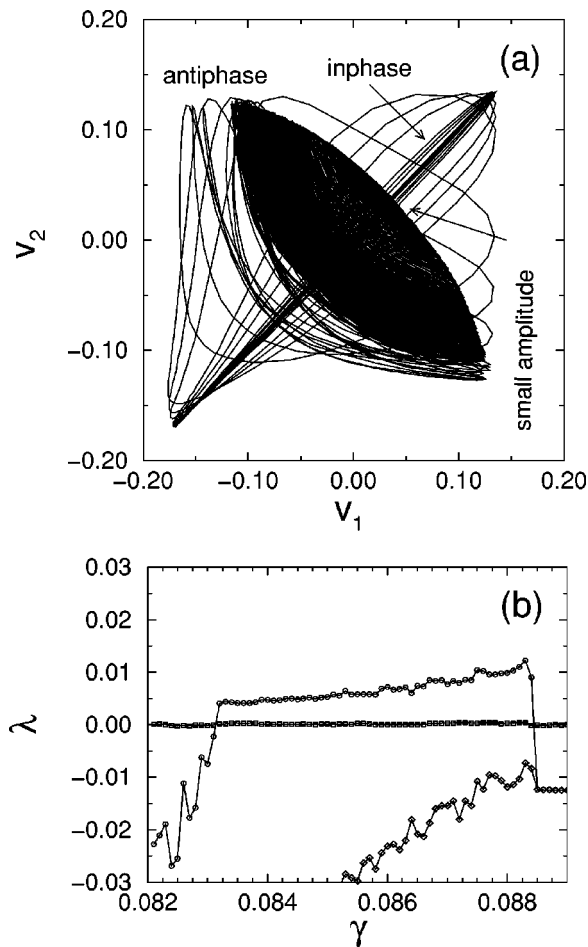


FIG. 3. (a) Projection of time trajectory onto (v_1, v_2) . For $J_1=J_2=0.075$ and $\gamma=0.084$, the trajectory sequentially passes through the stages of antiphase and in-phase oscillations as well as small amplitude stage. (b) Three largest Lyapunov exponents vs coupling strength γ . The chaotic behavior is observed for $\gamma \in (0.08315, 0.08841)$.

high-amplitude spiking, the medium-amplitude spiking, and nonspiking *silent* state in Fig. 2, respectively. Therefore, the chaotic bursting is composed of an itinerant process that traces from in-phase oscillation to antiphase oscillations, then to the silent state and back again to the in-phase oscillation.

Lyapunov exponents are plotted in Fig. 3(b) as a function of coupling strength γ . The largest Lyapunov exponent λ_1 has a distinctive positive value in the limited interval of $\gamma \in [0.08315; 0.08841]$, which implies that the bursting activity is chaotic. The abrupt change of λ_1 from negative to positive value indicates that the crises are the cause of transitions.

IV. FORMATION OF CHAOTIC ITINERANT STRUCTURE

As described in the preceding section, the chaotic bursting behavior is composed of three parts: the antiphase solution, the in-phase solution, and the silent state. It is quite interesting to understand how the chaotic behavior is suddenly generated from regular firing states and how the geometric manifold is organized to connect the three states.

In general, for two weak diffusively coupled oscillators, a pair of stable in-phase and unstable antiphase resonant solutions lies on the smooth torus. While for coupled ML systems, the antiphase solution is stable, with the in-phase solution unstable. As the coupling strength increases, the antiphase solution loses its stability and, as a consequence, the resonant torus structure will also be destroyed. The process of the resonant torus deformation across the boundary of the chaotic bursting region in Fig. 1 will clarify the mechanism underlying the birth of the chaotic bursting state. To construct the manifold structure where both the stable and saddle solutions lie, we use the numerical method suggested by Kevrekidis.²⁴ An ensemble of configurations is dispersed around the unstable in-phase solution. As the ensemble evolves for a long time, by plotting the Poincaré sections of the ensemble we obtain the underlying manifold structure.

In Figs. 4(a)–4(c), the Poincaré sections for $\gamma = 0.025, 0.08$, and 0.084 are presented, respectively. For weak coupling $\gamma = 0.025$, Fig. 4(a), an invariant closed curve is formed by the closure of the unstable manifold of the saddle in-phase solution I^+ to the stable manifold of the stable antiphase solution A . One unstable equilibrium point E^{++} and one of the unstable out-of-phase solutions U^{+++} are also plotted. The stability of equilibrium states and limit cycles are characterized by the superscript symbols “+.” The number of this symbol equals the number of unstable directions in phase space.

The closure of the invariant curve is smooth near the stable solution A in Fig. 4(a). With an increase of γ , the torus loses its smoothness due to wrinkling of the unstable manifold in the vicinity of the stable solution A . At $\gamma = 0.08315$, a saddle-node bifurcation for limit cycles occurs as the antiphase cycle A merges with the saddle cycle U^+ . The Poincaré section just before the bifurcation ($\gamma = 0.080$) is shown in Fig. 4(b). Crossing the bifurcation point ($\gamma = 0.084$), A is no longer an attracting set and becomes an attractor ruin. Although the trajectory stays for a long time at this point, it should leave the point for another solution. The problem is that there are no stable solutions. Instead, the equilibrium point E^{++} connects the disappeared cycle U^+ with saddle cycle I^+ . Then along the unstable manifold of I^+ , it is reinjected to the attractor ruin of A [Fig. 4(c)]. Thus the plot of manifold underlying the chaotic bursting state reveals that it has a chaotic itinerancy structure tracing the vicinity of I^+ , the attractor ruin of A , and the equilibrium point E^{++} and back again. Note that there is an alternative pathway from I^+ to A . Because symmetry of the system consisted of two identical oscillators, this pathway belongs to symmetric counterpart of the chaotic bursting solution illustrated in Fig. 4(c). Here and below, we focus on one of such itinerancy processes.

V. ALTERNATIVE ROUTE TO CHAOS VIA TORUS BREAKDOWN

Two coupled oscillators are synchronized when the frequency mismatch between two oscillators is not bigger than a certain limit that depends on the coupling strength. Typically, the synchronized zone, called a *resonant horn*, is bounded by two saddle-node bifurcation lines. Beyond these

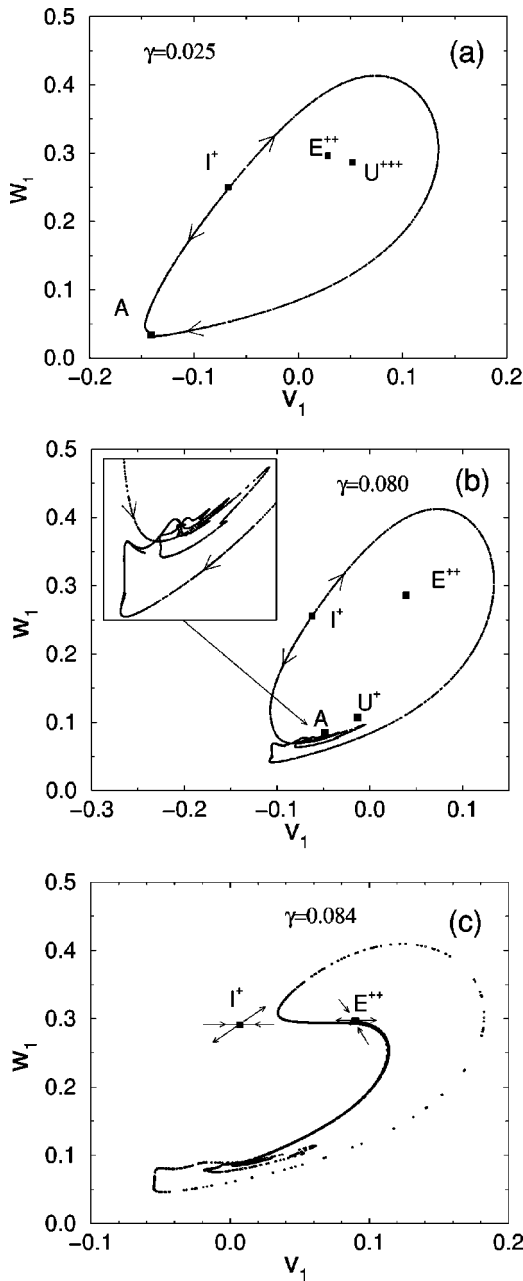


FIG. 4. (a) A Poincaré section for resonant torus with smooth closure of manifolds. (b) Development of wrinkling in the vicinity of the stable cycle. Folded structure is enlarged in the inset. (c) A Poincaré section for chaotic bursting.

lines, we have either a quasiperiodic, or a chaotic solution. Universal features of routes to chaos are characterized by the different schemes of the destruction of resonant torus. It is summarized by the Afraimovich–Shilnikov (AS) theorem.^{22,23} The possible routes to chaos via destruction of the resonant torus are (i) the saddle-node bifurcation of the stable resonant cycle and the saddle resonant cycle; (ii) the occurrence of the homoclinic structure involving both stable and unstable manifolds of the saddle resonant cycle; and (iii) the period doubling bifurcation of the stable resonant cycle.

The transition to chaotic itinerancy described in the preceding section looks similar to the AS scenario (i), but there are several differences. For a comparison, schematic illustra-

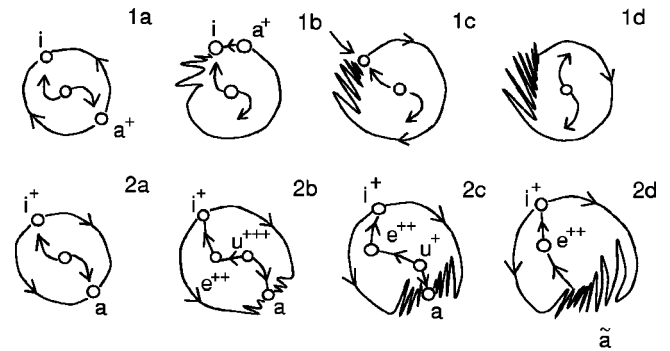


FIG. 5. Schematic diagrams illustrating deformation of manifold structure. In the top row, (1a)–(1d), AS scenario is presented. In the bottom row, (2a)–(2d), the Poincaré sections leading to chaotic bursting behavior for two diffusively coupled ML models are presented.

tions of the typical AS scenario (i) are plotted on the top row of Figs. 5(1a)–5(1d), while on the bottom row, Figs. 5(2a)–5(2d), the corresponding steps of the coupled ML system are plotted.

As shown in Figs. 5(1a) and 5(2a), the structures of the manifold at the tip of the resonant horns are very similar to each other except for the stability of two resonant cycles i and a . As expected, the invariant closed curve is smoothly formed by the closure of manifolds of resonant cycles.^{24,25} At least for weak coupling, the resonant cycles are accompanied by one unstable equilibrium point and two saddle limit cycles “inside” the torus. Two limit cycles do not play a role in the transition, hence are not denoted in Fig. 5. Note that for the coupled ML models, the antiphase solution a , rather than the in-phase solution i is stable.

The increase of coupling strength leads to formation of the folded structure near the stable resonant limit cycle [Figs. 5(1b) and 5(2b)]. In the ML system, however, there is one more event for the step (2a)→(2b). The unstable limit cycle u^{+++} appears from an equilibrium point e^{++++} via an inverse subcritical Hopf bifurcation, $e^{++++} \rightarrow e^{+++} + u^{+++}$. As a result, e^{+++} is a saddle–focus point whose stable manifold comes from u^{+++} , while the unstable manifold is connected to the stable manifold of saddle cycle i^+ .

For step (1a)→(1b), the control parameter is changed to move toward the boundary of the resonant horn. At the boundary of the resonant horn, the mutual convergence of the stable and saddle cycles leads to saddle-node bifurcation (1c). For step (2a)→(2b), let’s increase the coupling strength along the line $J_2 = 0.075$ in Fig. 1. At $\gamma = 0.08315$, a saddle-node bifurcation occurs (2c). Note that the unstable cycle u^{+++} undergoes an inverse torus bifurcation and becomes a saddle one, u^+ . And the saddle solution u^+ gradually converges to the stable resonant cycle a .

In case (1c), both the stable and the saddle limit cycles are lying on the torus surface while for case (2c), they are not. Both in (1c) and (2c), the stable resonant cycle disappears as a result of the saddle-node bifurcation and leaves an attractor ruin.

At the attractor ruin, the trajectory remains there for a long time, but finally escapes from the point along the unstable manifold. However, the fate of the escape from the

attractor ruin is quite different for two cases: For the AS scenario, (1d), the escaped trajectory rotates along the invariant closed curve and reinjected back to the position of the attractor ruin. Then the trajectory shows an intermittent chaos. For the ML system, (2d), as the stable cycle a annihilated with the saddle cycle u^+ , the trajectory at the attractor ruin, denoted as \tilde{a} , escapes from this point after a long transient period. The escape does not follow the former torus surface because the saddle cycle i^+ still exists. As the unstable manifold \tilde{a} , which inherits the disappeared cycle u^+ , is connected to the stable manifold of equilibrium point e^{++} , the escape from the \tilde{a} moves to e^{++} . After a transient period, along the unstable manifold of e^{++} , it moves toward i^+ . After another transient period at i^+ , the trajectory follows the unstable manifold of i^+ and reinjected into \tilde{a} . The itinerant trajectory tracing sequentially the antiphase, small amplitude, and in-phase states is responsible for the chaotic bursting behavior.

Let's consider the possibility of the chaotic itinerancy structure consisting of an attractor ruin of a stable in-phase solution and an unstable anti-phase solution in the two weakly coupled oscillators. As explained in the above, it is very evident that the AS scenario (i) is very different from the chaotic itinerancy structure observed in ML systems. While for the AS scenario (ii) and (iii), the local manifold structures near the in-phase solution are broken, but not the global manifold structures. Therefore, the appearance of the chaotic itinerancy is not expected.

VI. CONCLUSION

We have presented a coupled Morris–Lecar neuron model that shows chaotic bursting behavior. The time trajectory of the chaotic bursting state consists of three different parts: the high-amplitude oscillation, the medium-amplitude oscillation, and the nonfiring silent state. Numerical construction of manifold underlying the chaotic bursting state reveals there is a chaotic itinerancy structure that connects three unstable solutions: an antiphase synchronized solution, an in-phase synchronized solution, and an unstable equilibrium point. We have also shown that the route to chaotic bursting is different from the conventional Afraimovich–Shilnikov scenario of resonance torus breakdown. Therefore, the chaotic itinerancy will be an alternative route to chaos via resonant torus breakdown. As was shown recently, the chaotic itinerancy could be observed in higher dimensional systems with abundant unstable solutions.^{26,27} Therefore it will be very interesting to know how the chaotic itinerancy structure will persist in high-dimensional ML systems. The effect of the noise in the chaotic itinerancy will be also an interesting issue to be studied.

ACKNOWLEDGMENTS

We would like to thank Y. Kuramoto, C. Kurrer, H. Kook, and O. Sosnovtseva for discussions. This work was partly supported by the brain science research grant of the Ministry of Science and Technology, Korea. D.P. also acknowledges CRDF Grant No. REC-006 and RFBR Grant No. 01-02-16709.

- ¹B. Alving, *J. Gen. Physiol.* **51**, 29–45 (1968); M. Deschenes, J. P. Roy, and M. Steriade, *Brain Res.* **239**, 289–293 (1982).
- ²P. M. Dean and E. K. Matthews, *J. Physiol. (London)* **210**, 255–264 (1970).
- ³D. Hansel and H. Sompolinsky, *Phys. Rev. Lett.* **68**, 718–721 (1992).
- ⁴C. von der Malsburg and C. Schneider, *Biol. Cybern.* **54**, 29–40 (1986).
- ⁵C. A. Skarda and W. J. Freeman, *Behav. Brain Sci.* **10**, 161–195 (1987).
- ⁶M. C. Eguia, M. I. Rabinovich, and H. D. I. Abarbanel, *Phys. Rev. E* **62**, 7111–7122 (2000).
- ⁷I. Tsuda, *Behavior Brain Sci.* **24**, 793–847 (2001).
- ⁸J. Rinzel, in *Ordinary and Partial Differential Equations*, edited by B. D. Sleeman and R. J. Jarvis (Springer-Verlag, Berlin, 1985), pp. 304–316; in *Mathematical Topics in Population Biology, Morphogenesis and Neuroscience*, edited by E. Teramoto and M. Yamaguti (Springer-Verlag, Berlin, 1987), pp. 267–281.
- ⁹E. M. Izhikevich, *Int. J. Bifurcation Chaos Appl. Sci. Eng.* **10**, 1171–1266 (2000).
- ¹⁰S. K. Han, C. Kurrer, and Y. Kuramoto, *Phys. Rev. Lett.* **75**, 3190–3193 (1995).
- ¹¹A. Sherman and J. Rinzel, *Proc. Natl. Acad. Sci. U.S.A.* **89**, 2471–2474 (1992).
- ¹²D. Postnov, S. K. Han, and H. Kook, *Phys. Rev. E* **60**, 2799–2807 (1999).
- ¹³I. Tsuda, E. Korner, and H. Shimizu, *Prog. Theor. Phys.* **78**, 51–71 (1987).
- ¹⁴K. Ikeda, K. Otsuka, and K. Matsumoto, *Prog. Theor. Phys. Suppl.* **99**, 295–324 (1989).
- ¹⁵K. Kaneko, *Physica D* **41**, 137–172 (1990).
- ¹⁶C. Morris and H. Lecar, *Biophys. J.* **35**, 193–213 (1981).
- ¹⁷A. L. Hodgkin and A. F. Huxley, *J. Physiol. (London)* **117**, 500–544 (1952).
- ¹⁸For the single Morris–Lecar model $J_{ion}(v, w) = \bar{g}_{Ca}m_{\infty}(v)(v - v_{Ca}) + \bar{g}_K w(v - v_K) + \bar{g}_L(v - v_L)$, $m_{\infty}(v) = 0.5[1 + \tanh\{(v - v_a)/v_b\}]$, $w_{\infty}(v) = 0.5[1 + \tanh\{(v - v_c)/v_d\}]$, $\tau_w(v) = 1/\cosh\{(v - v_c)/(2v_d)\}$. Typically used parameter values are $v_a = -0.01$, $v_b = 0.15$, $v_c = 0.1$, $v_d = 0.145$, $\bar{g}_{Ca} = 1.0$, $\bar{g}_K = 2.0$, $\bar{g}_L = 0.5$, $v_{Ca} = 1.0$, $v_K = -0.7$, $v_L = -0.5$, and $f = 1.15$. See also Refs. 16 and 10.
- ¹⁹C. Grebogi, E. Ott, and J. A. Yorke, *Phys. Rev. Lett.* **48**, 1507–1510 (1982).
- ²⁰Y.-C. Lai, C. Grebogi, and J. A. Yorke, “Sudden change in the size of chaotic attractors: how does it occur?” in *Applied Chaos*, edited by J. H. Kim and J. Stringer (Wiley, New York, 1992).
- ²¹D. Postnov, S. K. Han, O. Sosnovtseva, and C. S. Kim, *Diff. Eq.* **10**, 115–149 (2002).
- ²²V. I. Arnol'd, V. S. Afraimovich, Yu. S. Il'yashenko, and L. P. Shil'nikov, *Dynamical Systems, Vol. 5, Bifurcation Theory and Catastrophe Theory* (Springer Verlag, New York, 1994).
- ²³V. S. Anishchenko, *Dynamical Chaos—Models and Experiments: Appearance Routes and Structure of Chaos in Simple Dynamical Systems* (World Scientific, Singapore, 1995).
- ²⁴I. G. Kevrekidis, R. Aris, and L. D. Schmidt, *Physica D* **23**, 391–395 (1986).
- ²⁵I. G. Kevrekidis, L. D. Schmidt, and R. Aris, *Chem. Eng. Sci.* **41**, 1263–1276 (1986).
- ²⁶K. Hashimoto and T. Ikegami, *J. Phys. Soc. Jpn.* **70**, 349–352 (2001).
- ²⁷M. Komuro, “A mechanism of chaotic itinerancy in globally coupled maps,” preprint, 2002.